



# Adaptive eyeglasses for presbyopia correction: an original variable-focus technology

JESSICA JAROSZ,\* NORBERT MOLLIEX, GUILHEM CHENON, AND BRUNO BERGE

Laclarée, 9 rue du Vercors, 69007 Lyon, France

\*[jessica.jarosz@laclaree-vision.com](mailto:jessica.jarosz@laclaree-vision.com)

**Abstract:** We propose an original variable-focus technology specially designed for presbyopia-correcting adaptive eyeglasses. It has been thought through to offer vision comfort without cutting on aesthetics. It relies on a fluid-filled variable-focus lens (presenting 2 liquids and 1 ultra-thin membrane) assisted by a low-power and high-volume microfluidic actuator. It also features a distance-sensing system to provide automatic focusing. We demonstrate the qualities of this novel technology on our first prototype. Our prototype achieves the necessary 3-diopter-high power variation on a 20-millimeter-wide variable zone with low actuation pressures ( $\sim 200$  Pa at most), and the preliminary optical quality analysis shows the spatial resolution is much better than the one specified by classic eye charts. We discuss further improvements in terms of optics, aesthetics and portability. In particular, we point out that this variable technology is compatible with standard base curves, and we highlight an optimal configuration where the power consumption of our opto-fluidic engine is about 25 mW peak.

© 2019 Optical Society of America under the terms of the [OSA Open Access Publishing Agreement](#)

## 1. Introduction

Presbyopia is a visual impairment caused by the normal aging of the crystalline lens and resulting in progressive loss of accommodation [1]. As a consequence, from the onset of presbyopia occurring around 40–45 years old, the eye has growing trouble focusing at near and intermediate distances. At around 55–60, the eye is fully presbyope and can no longer focus on close objects [2, 3]. There are about 1.8 billion presbyopes in the world [4]. Considering North America, Europe and Japan alone, more than 400 million are concerned for about half of their lives, and the prevalence is increasing because of population aging.

Going through presbyopia is more or less painful, in any case, it does affect quality of life [5–7]. Eyeglasses are by far the most popular solution to presbyopia correction. Current widespread solutions all consist in static lenses and today, the best compromise solution is progressive addition lenses (PALs); these multifocal lenses offer a vertical gradient of power addressing all vision distances within a single lens. The alternative solution is multiple single vision eyeglasses, which is not very convenient.

There is a need for novel means of presbyopia correction [8] because PALs do not fit everyone. Some presbyopes give them a try and reject them. Some presbyopes cannot be prescribed them, e.g. because of heterophoria, significant convergence insufficiency or anisometropia [9] (i.e. significant refractive error difference between both eyes). Among PAL wearers, either equipped with conventional or personalized progressive lenses coming out of the state-of-the-art lens technology [10], some presbyopes are unsatisfied with their vision: between 6% [11] and 14% [12] of PAL wearers would be unsatisfied. Customized PALs give better satisfaction over conventional ones [12–14], providing that they are well adjusted (their performance is indeed very sensitive to mounting errors). However, there are intrinsic limitations to PAL technology: it generates unwanted astigmatism [15] and restricts the field-of-vision attributed to each vision distance (as each lens power is assigned a defined bounded lens area), especially the one that is

attributed to intermediate powers which is confined to a narrow corridor [16]. Besides, for some presbyopes, the ergonomics of PALs relying on changing gaze directions to get clear vision just might not fit their need [8] or might be inadequate [17]. Computer vision is one of the issues with general purpose PALs as they often offer limited field-of-vision at intermediate distances and can decrease reading speed [18]. So as to bypass the limitations of PALs at intermediate powers, occupational progressive lenses offering clear vision from intermediate to near vision (but no clear distance vision) are proposed. They are indeed better rated for computer work [19, 20] but overall satisfaction is hampered by their being deprived of distance vision [20].

A static lens cannot fully correct presbyopia. In addition, it has to be renewed at each adjustment of the addition and each stage of presbyopia. The most straightforward solution to presbyopia correction would be to make the wearer retrieve the auto-focus function of the crystalline lens fading away with age with a variable-focus lens; there have been numerous developments for about half a century towards such a lens [8]. Providing that this lens is technically feasible, it also appears as rather simple to dispense as opposed to PALs which present a very large variety of designs [21] and for which adaptation can be difficult [17].

Several variable-focus technologies have been considered so far for adaptive eyeglasses. One of the first attempts was fluid-filled lenses comprising 1 deformable membrane and 1 liquid [22]. These lenses feature a large dioptric range due to the significant refractive index difference between liquid and air. Successful developments of these fluid-filled lenses have been achieved for one-time adjustable lenses based on Joshua Silver's pioneering work aiming at providing a low cost and self-refraction solution to ametropes in developing countries [23]. As regards real-time adaptive correction, as for presbyopia correction, considering the aesthetics and optical standards on eyewear, the membrane lying at the liquid-air interface raises a difficult compromise between the optical quality of the lens and the requested deformation forces in relation to the weight, size and electrical consumption of the actuation system. As a consequence, liquid-membrane-air fluid-filled lenses are often operated by manual actuation [24]. More recently, Hasan *et al.* managed to develop a prototype of eyeglasses featuring liquid-membrane-air fluid-filled lenses using a piezoelectric actuation system – the system remains bulky [25]. Several groups have explored a liquid-membrane-liquid structure to reduce the gravity effect and obtain a good optical quality [26, 27]. Electrowetting lenses based on 2 immiscible fluids actuated by electrostatic forces have also been examined as a possible solution for variable-focus spectacles [28]. Given their low power consumption and high optical quality, electrowetting lenses are well suited for contact or intraocular lenses but they do not appear well adapted for large diameter lenses, because the specification on density matching of both liquids gets too demanding. An alternative variable-focus technology is proposed by the Alvarez lenses [29], where 2 optical components with complex surfaces are superimposed and laterally translated so as to produce the needed change of optical power. On such device, the stack of lenses present multiple air-lens interfaces and is usually visible on the edge, besides, the implementation is manual [30]. Since the 1980s, liquid crystal (LC) lenses have been investigated as well. LCs can change the index of refraction of a transparent medium through re-alignment of polarizable molecules under an E-field [31]. Based on that principle, several concepts of variable-focus lens were designed: parabolic gradients, solid profiles immersed inside the LC [32], and more recently, reconfigurable diffractive optics [33]. This technology route could appear attractive as the LC technology has matured for more than 40 years in the display industry. Nevertheless all these concepts share major drawbacks when considering presbyopia correction. First, working in unpolarized light generally requires doubling the stack of layers – one for each E-field direction. Also, LCs have very limited phase shifts due to the thickness of the molecular layer, so diffractive lenses are used to bend the light, which increases the risk of getting energy in un-wanted diffraction orders, thereby decreases contrast and bringing flares.

This paper describes an original opto-fluidic engine implementing a variable fluid-filled lens,

comprising an ultra-thin membrane sandwiched between 2 different refractive index liquids, and actuated by a low-power high-volume microfluidic pump. This presbyopia-correcting adaptive doublet lens is circular and embedded within an ophthalmic lens of any external shape which provides the static refractive correction. We will demonstrate how this novel variable-focus technology is relevant for adaptive eyeglasses aimed at presbyopia correction. First of all, in Sect. 2, we will summarize the specifications on presbyopia-correcting adaptive lenses. Then, in Sect. 3, we will show how a fluid-filled lens can comply with all the optical, aesthetics and portability requirements on such eyeglasses and in Sect. 4, we will report the performance of our first prototype. Finally, in Sect. 5, we will present how the performance of the next generation of prototypes will be improved.

## 2. Requirements for presbyopia-correcting adaptive lenses

### 2.1. Addition

The necessary power addition to correct near vision depends on the remaining subjective amplitude of accommodation, the desired working distance and the visual needs (task size). The amplitude of accommodation determines the nearest point at which an object may be viewed. After about 55-60, true accommodation exerted by the lens has disappeared [2, 3] and the residual subjective accommodation is then mainly based on the depth-of-focus of the eye [34], which is related to pupil diameter, ocular aberrations as well as psychological factors. The near addition should provide a location of the nearest point between 20 cm and 30 cm to ensure comfortable vision [35]. The usual range of near addition goes from 0.75 D at around 40 up to 3 D at around 70; superior addition can be prescribed in case of short working distance or reduced visual acuity.

Adequate near addition is essential to visual comfort. However, addition needs regular adjusting that is why it should be kept adjustable. First, its determination can be plural so it may need adjusting after practical testing. Indeed, the nearest point measurement depends on a number of factors such as pupil size and task illumination. Also, to prevent from eye strain, it has been suggested that functional presbyopes should keep a part of their accommodation amplitude in reserve but this part is not well defined [34, 36]. Second, requested addition can rapidly evolve with age. Hofstatter *et al.* measured a decrease in the amplitude of accommodation as high as -0.3 D per year during presbyopia [37].

### 2.2. Static correction

Static spherocylindrical refractive errors must be corrected to enjoy clear vision at all distances. At close distances, the spherical equivalent results from the sum of the static spherical equivalent and of the addition.

As the accommodation ability decreases the eye tends to appear more and more hyperopic, because the accommodation system is characterized by over-accommodation for far targets [38]. Nevertheless, this drift is very little (about -0.04 D per year [8]). Therefore, it does not request to implement an adjustment of the sphere in the adaptive lenses over a typical eyeglass lifetime.

### 2.3. Focusing response

Targeting the natural pre-presbyopic accommodative response seems a safe bet. Consequently, the focusing response should be, first, continuous (at least pseudo-continuous, as long as focus changes are not perceivable to the eye), second, automatic with an auto-focusing error inferior to the eye's depth-of-field (about 0.5 D total for a person aged 45-70 and a light-adapted value of pupil diameter) and last, as quick as before presbyopia. Concerning, the temporal response, on the one hand, the response time should be quick enough to be safe and enjoy visual comfort; on the other hand, it should not be too quick to avoid bothering noticeable modifications in magnification due to the power change of adaptive lenses. Total natural response time to switch between far

vision and near vision, including both reaction time (300 to 400 ms) and accommodation time (400 to 1000 ms), amounts to about 1 s [39–41] for non-presbyopic adults.

The best focusing response in terms of vision comfort is not easy to predict, in particular for functional presbyopes who still have a remaining accommodation ability. The wearer would benefit from a preliminary test assessing the most adapted focusing response.

#### 2.4. *Field-of-vision of the variable zone dedicated to near and intermediate visions*

Near and intermediate visions have become more and more important; a recent study showed that today about 60 % of Americans spend more than 5 hours a day in front of a screen and 30 % more than 9 hours a day [42]. As a consequence, it is crucial to ensure presbyopes a comfortable field-of-vision in front of screens. In terms of field-of-vision, a 5-inch diagonal smartphone screen (among the largest available as regards smartphones) located at 30 cm from the eye (preferred near vision distance [43]) corresponds to  $\pm 11^\circ$  and a 27-inch diagonal computer screen (among the largest available as regards computers) located at 63 cm from the eye (preferred intermediate distance [44] and recommended minimum distance for a computer screen [45]) to  $\pm 28^\circ$ . Viewing a large computer screen at intermediate distance seems one of the most field demanding tasks at intermediate vision therefore it is a good starting point to specify the requested field-of-vision.

#### 2.5. *Optical quality*

Optical quality is decisive and comprises high transmission, good wavefront error, no troublesome scotoma (blind area). The lenses should be able to feature available surface treatments and should be curved to optimize off axis aberrations [46] in distance vision and minimize specular reflections.

#### 2.6. *Aesthetics and portability*

The eyeglasses should be ordinary looking: acceptable volume of the eyeframe, any shape of the lens contour, large aperture, curved lenses. The weight is important. Besides discomfort, heavy eyeglasses (over 60 g) can cause injury, e.g. nasal dermochalasis – excess skin entailed by heavy skin stretching [47]. Typical eyeglasses weigh in the range of about 7-50 g. To provide all-in-one everyday eyeglasses, minimal autonomy should be more than 20 h, allowing overnight recharging. Electronic energy consumption and weight budget for the battery are closely linked together. As a rule of thumb, a few grams of battery are allowed on each side of the eyewear frame, not much more.

### 3. Design principle

Previous developments of variable fluid-filled lens [25, 26] demonstrated that it was possible to achieve the 3-diopter-high power variation that is necessary to correct for presbyopia with a reasonable optical quality. However, it is essential to take into account the additional aesthetics, ergonomics and portability requirements as well. This led us to reconsider the design of such lens and, most importantly, the actuation approach.

#### 3.1. *Lens design*

The design of our variable-focus lens is sketched on Fig. 1, it can be either plano or curved, thus meeting the ophthalmic eyeglass standards. It is a 4 layer lens. The 2 middle layers form the central doublet lens and provide the addition. The 2 external layers enclose the system, provide the static correction and incorporate the desired lens treatments. The central doublet lens features a variable focus over a large circular zone. In this zone, it comprises 2 fluid layers with different refractive indexes (a low-index layer and a high-index layer) separated by an ultra-thin deformable membrane: these form the variable fluid-filled lens. The general underlying principle consists

in changing the optical power by changing the shape of the refractive surface between the 2 fluids by deforming the membrane, which implies varying the volume ratio of the 2 fluids in the lens. Outside the variable zone, there is no dioptric change, the layers are formed by both fluid and solid materials and feature transport channels to carry the fluids from the actuation system to the variable zone. The external lens contour can thus be of any shape. The boundaries of the adaptive doublet lens and of the transport channels are by design not visible. Besides, the curvature of the membrane matches the one of the outer part when no addition is provided.

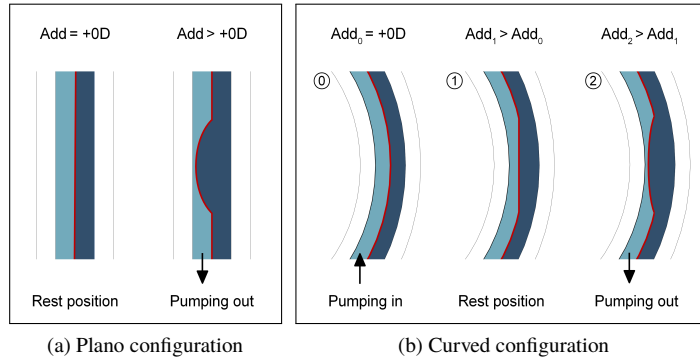


Fig. 1. Schematic of the variable-focus lens. It can be either plano (a) or curved (b). The light blue layer refers the low-index layer and the dark blue layer to the high-index layer. The membrane is figured in red at the interface between both layers. In the plano configuration, when no liquid pressure is applied, the addition  $Add$  provided by the doublet lens is 0 D; when fluid is pumped out of the low-index layer, the addition increases. In the curved configuration, when no liquid pressure is applied, the addition provided by the doublet lens is positive; when fluid is pumped into the low-index layer, the addition decreases and when fluid is pumped out of the low-index layer, the addition increases.

We define the base curve of the variable lens in relation to the radius of curvature of the outer part of the central refractive surface of the doublet lens (that is fix). So that readers can quickly relate to the classic definition of the base curve given for a simple ophthalmic lens, in our calculations of the base curve, we considered a refractive surface separating air and a medium with a refractive index of 1.530 (the standard tooling index, which is commonly used in the ophthalmic industry [46]).

### 3.2. Soft actuation approach

The elastic membrane deformation results from the balance between the tensile forces and the pressure force induced by the liquid. In case gravity forces are negligible and the membrane features a uniform thickness, elastic deformation of a membrane clamped at a circular boundary can be approximated by a sphere of radius  $R$  as long as deformations are small as compared to the lens aperture size [48]:

$$\frac{1}{R} = \frac{\Delta P}{2T}, \quad (1)$$

where  $\Delta P$  is the liquid pressure and  $T$  the lateral tension of the membrane. As illustrated on Fig. 1, when the actuator is pumping fluid into the low-index layer, the membrane tends to spherically bulge outward and when the actuator is pumping fluid out of the low-index layer (or pumping into the high-index layer), the membrane tends to cave in in the opposite direction. Given the refractive index difference between the 2 fluids forming the doublet, the optical power

of the adaptive doublet lens  $P_{opt}$ , that is the addition, can be directly derived from the volume of the spherical cap defined by the membrane, and, the axial displacement of the membrane, which defines the minimal thickness of the doublet liquid lens, from the sag of the spherical cap. Figure 2 shows the requested volume to achieve a power variation from 0 to 3 D as a function of the adaptive lens aperture for several values of refractive index difference – a 0.2 refractive index difference has previously been reported [26] and the refractive index difference between 2 optical fluids can hardly be pushed above 0.4 [49]. Following our examination of the requested field-of-vision in Sect. 2.4, from now on, we will consider a lens diameter of 20 mm, which provides a 65° field-of-vision. The volume to be displaced would be from 75  $\mu\text{L}$  ( $\Delta n = 0.3$ ) to 250  $\mu\text{L}$  ( $\Delta n = 0.1$ ) and the thickness of such a lens would be from 0.5 mm ( $\Delta n = 0.3$ ) to 1.5 mm ( $\Delta n = 0.1$ ).

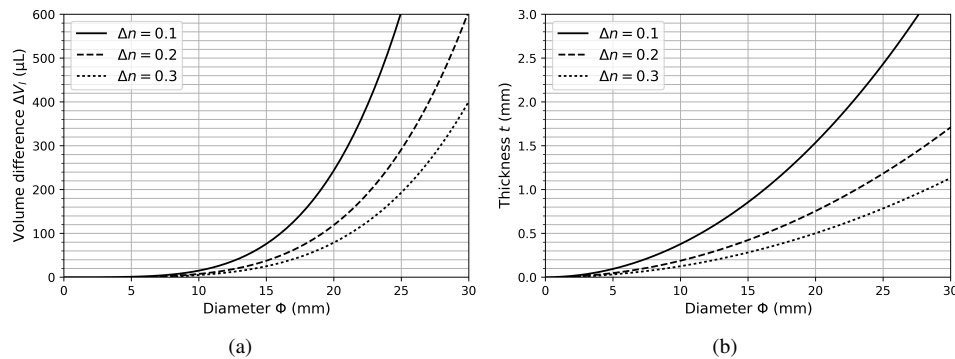


Fig. 2. Volume to be displaced (a) and minimal thickness (b) of the adaptive doublet lens providing a power variation from 0 to 3 D.

In order to achieve a good optical quality, the pressure gradient generated by gravity due to the liquid density difference has to be negligible as compared to the pressure due to the elastic force exerted by the membrane. In terms of aperture, it means that the capillary length has to be much larger than the variable lens aperture, the capillary length being given by  $\lambda_c = \sqrt{\frac{T}{\delta\rho g}}$  where  $\delta\rho$  is the density difference between both liquids,  $T$  is the lateral tension of the membrane and  $g$  is the gravitational acceleration. For a 20 mm diameter lens, considering for instance the density of water for the low-index liquid and a 5 % liquid density difference, the threshold value of the lateral tension below which the gravity force degrades optical quality would be about 3 N/m.

Under deformation, the lateral tension of the membrane can be expressed by:

$$T = T_0 + \frac{eE}{2(1-\nu)} \cdot \frac{dA}{A}, \quad (2)$$

where  $T_0$  corresponds to the lateral tension of the membrane at rest (when the membrane is plane),  $\frac{dA}{A}$  to the relative surface increase,  $e$  to the thickness of the membrane,  $E$  to the Young's modulus and  $\nu$  to the Poisson coefficient. Thus, the requested fluidic pressure as a function of the optical power is given by:

$$\Delta P = \frac{2T_0}{\Delta n} \cdot P_{opt} + \frac{eE\Phi^2}{16(1-\nu)\Delta n^3} \cdot P_{opt}^3, \quad (3)$$

with  $\Delta n$  the refractive index difference between both fluids and  $\Phi$  the diameter of the variable zone. Therefore, low actuation pressure is associated with thin membrane, low material stiffness

and low initial lateral tension of the membrane. For a minimal lateral tension of 3 N/m and a 0.2 refractive index difference, linearization of Eq. (3) gives a required fluid pressure to provide for the 3 D addition (in the plano configuration) of about a hundred Pascals; for such a lateral tension, no matter how thin the membrane and how low its stiffness, the required fluid pressure will not be inferior to this. This sets the requested maximum actuation pressure to a few hundreds Pascals.

In order to provide the requested volume and pressure detailed above while consuming little energy, a novel concept of high-volume and low-power microfluidic pump based on electrostatic actuation was developed [50,51]. The variable-focus system comprising the actuator and the lens forms the opto-fluidic engine. The actuator relies on a slack metallized film which is confined between 2 grid-electrodes separated by a gap. The film separates 2 fluids, each is connected to one of the lens fluid layers. The system is running at constant overall volume. The application of a voltage difference between the film and one of the grid-electrodes makes the film move towards this electrode and sweeps the fluid lying between the film and this grid-electrode off the pump, while the other fluid is drawn in to fill the gap between the film and the other grid-electrode. The actuator is bidirectional as the film can be attracted by both grid-electrodes. Thus it can deliver both negative and positive differential pressures. The differential pressure between both fluids is by convention positive when an increase of the lens optical power is entailed. We showed elsewhere that the differential pressure  $\Delta P_{pump}$  can be modeled by a quadratic function of voltage  $V$  [51]:

$$\Delta P_{pump} = k \cdot V^2, \quad (4)$$

where  $k$  is a constant depending on the design parameters of the actuator. For example, this pump can provide an actuation pressure of 200 Pa (on each side of the actuator, that is an actuation pressure range of [-200 Pa, 200 Pa]) and an exchanged volume of 100  $\mu\text{L}$  for a voltage of 100 V, these characteristics being adjustable with the design parameters. Furthermore, electrically, this actuator can be viewed as a capacitance whose measurement is directly correlated to the exchanged volume, in other words to the adaptive lens power.

### 3.3. Response time

When the actuator is pumping, the transient state describing the differential pressure across both sides of the lens membrane  $\Delta P$  over time  $t$  is described by:

$$\Delta P = \Delta P_{pump} - Q \frac{dV_l}{dt}, \quad (5)$$

where  $V_l$  is the volume that has been displaced and  $Q$  the fluidic impedance; the fluidic impedance being due to the liquid viscosities, the geometry of the transport channels (in the actuator, in the lens and in between) and of the actuator grids. We considered the first order expansion of  $\Delta P(V_l)$ . Provided that the radius of curvature of the membrane is very large as compared to the deformation and to the aperture size, the steady state response of the lens is given by:  $\Delta P = \frac{128T}{\pi\Phi^4} V_l$ , where  $T$  is the lateral tension of the membrane and  $\Phi$  the lens aperture. As long as the lateral tension does not vary much over the deformation, Eq. (5) can be rewritten as:

$$Q \frac{dV_l}{dt} + \frac{128T_0}{\pi\Phi^4} V_l = \Delta P_{pump}, \quad (6)$$

The solution of this differential equation is a decaying exponential function whose time constant is  $\tau = \frac{\pi Q \Phi^4}{128 T_0}$ . This result enables a simple modeling of the response time of the lens, according to basic system parameters which can be easily measured. The lower the friction loss and the higher the lateral tension of the membrane, the lower the response time of the lens. Yet, it has to be noticed that this result is only valid for small steps around the rest position of the membrane.

## 4. Experimental demonstration of our variable-focus technology for presbyopia correction

### 4.1. Description of the demonstrator

A prototype was set up to demonstrate the potential of this variable-focus technology. This prototype is not miniaturized but it is portative. As depicted on Fig. 3, it features:

- 2 opto-fluidic engines, 1 for each eye,
- a distance sensor, delivering a measurement of the focusing distance of the wearer,
- a control system, calculating the necessary addition and driving the opto-fluidic engines; the system can also be operated in manual mode (then the operator can switch between 3 selected additions corresponding respectively to distance, intermediate and near visions).

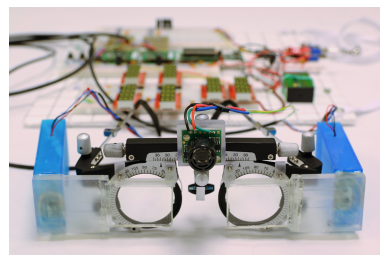


Fig. 3. Photograph of the prototype.

The opto-fluidic engines as well as the distance sensor are integrated on the eyeglass frame which is a mere trial lens frame. The lens is connected to the actuator via a 90° angled 3D-printed connector so that the actuator can be positioned at the eyeglass arm level. The internal section of this connector is  $\sim 5 \times 3 \text{ mm}^2$  for both transport channels. The actuators are inserted in a protecting housing (the blue boxes on the picture). The distance sensor is placed on the eyeglass bridge. The control system and the battery are gathered on a remote portable miniboard connected to the prototype with a 1-meter long 12 wires cable. The ergonomics of the prototype is basic, yet it enables to adjust the lens centering (interpupillary distance, height) and correct the wearer's static correction by inserting trial lenses on the back side of the frame.

#### 4.1.1. The opto-fluidic engine

##### 4.1.1.1 The variable-focus lens

We present a plano variable-focus lens. The adaptive doublet lens features a 20 mm diameter and a 0.2 refractive index difference. The whole lens is  $30 \times 40 \text{ mm}^2$  and about 4 mm thick. The general structure was detailed in Sect. 3.1 and our realization is outlined on Fig. 4 (solid structure). The static power of the lens (i.e. the power in rest state, which is associated with a plane configuration of the membrane) is 0 D.

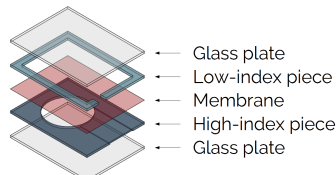


Fig. 4. Layout of the solid structure of the variable-focus lens.

The 2 external lenses consist of flat 1mm-thick borosilicate glass plates. The solid parts in the central doublet lens are made of UV cured resins and formed using elastomeric molds. There are on the one hand, a high-index piece (in dark blue on Fig. 4) belonging to the high-index layer, and on the other hand, a low-index piece (in light blue on Fig. 4) belonging to the low-index layer. The high-index piece is basically a plate with a 20 mm diameter circular hole which defines the variable zone. This piece exhibits a local depression going from the hole to the edge of the piece that constitutes the transport channel for the circulation of the high-index fluid. The planar part of the high-index piece supports the optical membrane which is bounded to it using a UV cured adhesive. The membrane is based on a soluble fluorinated polymer; such material was previously implemented in thin free-standing membranes [52] and in the context of variable-focus optics [53]. On the top of this assembly, a low-index cavity that is larger than the hole of the high-index piece is placed and glued. The low-index piece comprises a transport channel as well, but contrary to the high-index channel, it extends over the whole thickness of the low-index layer. Each cavity is filled with 1 liquid: the cavity of the low-index piece is filled with the low-index liquid and the cavity of the high-index piece is filled with the high-index liquid. So that the solid-liquid interfaces may not be visible, the refractive indexes of the high-index and low-index liquids match the one of the high-index and low-index pieces, respectively. We worked with a density mismatch between both liquids better than 5 %. Candidate liquids can be chosen among the thousands of transparent organic molecules which are liquid at room temperature. Ober *et al.* provided much valuable information regarding liquids selection [49]. The materials that we use are detailed in [54].

The membrane is made by spin coating on a wafer which has previously been coated with a sacrificial layer. A conventional spin profile was implemented (speed: 4000 rpm for 30 s, acceleration: 1000 rpm/s for 4 s). After complete heat evaporation of the solvent, the membrane is attached on a temporary supporting frame for practical manipulation, before being freed from the substrate by dissolution of the sacrificial layer. Several polymer concentrations were tried to adjust the lateral tension. The thinner the membrane, the lower the lateral tension. The specifications on the lateral tension and on the actuation pressure (cf. Sect. 3.2) led us to a membrane thickness of 350 nm, obtained for a polymer concentration of 3 wt%.

The optical power characterization of our variable-focus lens as a function of the differential pressure between the 2 fluid layers is shown on Fig. 5. The optical power is here measured in air that is to say before fluid filling. The measurements result from a magnification analysis of images coming from the optical reflection on the membrane. For clarity, the experimental data are scaled by  $\Delta n/2$  to simulate the optical power values of the lens once it is filled in with liquids. A homemade pressure generator regulating the differential pressure is used. It consists of a motorized syringe able to inject/retract well defined volumes of air in a large chamber. The pressure generator is connected to the high-index layer while the low-index layer is left open to room air pressure. A differential pressure sensor (Omega, PX163) monitors the corresponding generated differential pressure. We fit the experimental data with the theoretical model provided by Eq. (3). The polynomial function fits well with the experimental data. It gives a lateral tension of the membrane of 4 N/m and a Young's modulus of 2 GPa. In this experimental configuration (plano lens), the [0, 3 D] requested addition range is obtained for an actuation pressure range of [0, ~200 Pa], which is in line with the performance of the actuator.

#### 4.1.1.2 The high-volume and low-power actuator

The total dimensions of the pump are about  $55 \times 18 \times 7 \text{ mm}^3$ . As detailed in Sect. 3.2, each actuator features 3 electrodes (one can actually see 3 wires going out of the blue protective housings containing the pumps on Fig. 3): V+ and V- relate to the 2 grid-electrodes, and COM to the film. Connecting the voltage source to COM/V+ will apply a positive differential pressure between the high-index and low-index fluid layers whereas connecting the voltage source to COM/V- will apply a negative differential pressure. For clarity, on the following graphs, positive

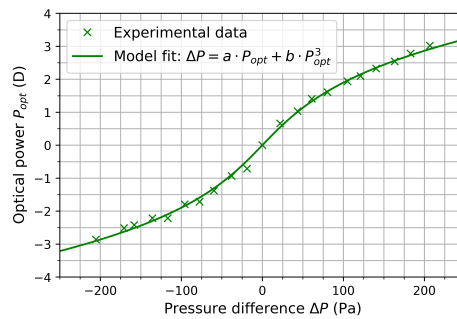


Fig. 5. Typical power response of the variable-focus lens obtained before fluid filling. Experimental data (green 'x' markers) is presented along with model fit based on Eq. (3) (green solid line).

voltages and negative voltages refer to COM/V+ voltages and to COM/V- voltages, respectively. This voltage sign convention is linked to the liquid flow direction, but it is not related to the sign of the applied voltage. With this convention, positive voltage tends to increase optical power, whereas negative voltage does the opposite. In any case, voltages are here AC voltages, with no polarity.

#### 4.1.2. The distance sensor

A simple ultrasonic range-meter (Maxbotics MB1030) based on the time of flight of ultrasounds (US) is used to assess the focusing distance of the wearer. These sensors use a single transducer for emission and reception. They are easy to operate and the limited repetition rate (50 ms per measurement) is high enough for our purpose (we only need to measure distance up to 4 m maximum). The angular cone of measurement is approximately  $\pm 20^\circ$ , although it is varying with target size and distance.

#### 4.1.3. The control system

A simple microcontroller (Microchip PIC24FV16KM202) is controlling the prototype. After measuring the distance to the front scene, the microcontroller calculates the voltages to be applied to each microfluidic actuator, using a simple calibration table giving the optical power as a function of voltage on each opto-fluidic engine. Then the microcontroller sends the information to 2 commercial drivers (MAX14521E). These commercial drivers have been designed to drive electroluminescent sheets and are well adapted to a capacitance load of up to several tens of nanofarads. The output generates an alternative voltage (0 – 140 Veff, 100 Hz in our case) with a square shape and transition fronts that are typically shorter than 10 % of the period. The driver features 4 independent outputs, allowing to use only 1 driver for both sides of each actuator, and potentially 1 driver for both eyes. Power consumption of the drivers is roughly a quadratic function of voltage, it typically amounts to 100 mW at maximum voltage (140 V) on our actuator.

### 4.2. Optical performance of the prototype

#### 4.2.1. Optical power response

The optical power response of the opto-fluidic engine (filled with liquids) as a function of voltage is given on Fig. 6(a). The measurements result from a magnification analysis based on images of a grid acquired through the lens. The opto-fluidic here integrates the variable lens whose characterization was presented on Fig. 5. The figure shows that the opto-fluidic engine manages to achieve the necessary 3-diopter-high addition with an input voltage delivered by the selected

drivers. As expected, the response is non-linear. The experimental data are compared to the model data (figured by the solid lines) obtained from Eqs. (3) and (4), considering the experimental parameters of the opto-fluidic engine. The thresholds indicated on the model data highlight the maximum volume that can be displaced by the pump integrated in the opto-fluidic engine, according to the experimental estimation of the maximum active volume of the actuator [51], which seems a little under-estimated here. Both the experimental and model data are in accordance on the overall tendencies: dioptric range, quadratic dependency of optical power with voltage at low voltages, saturation when the maximum volume of liquid has been moved.

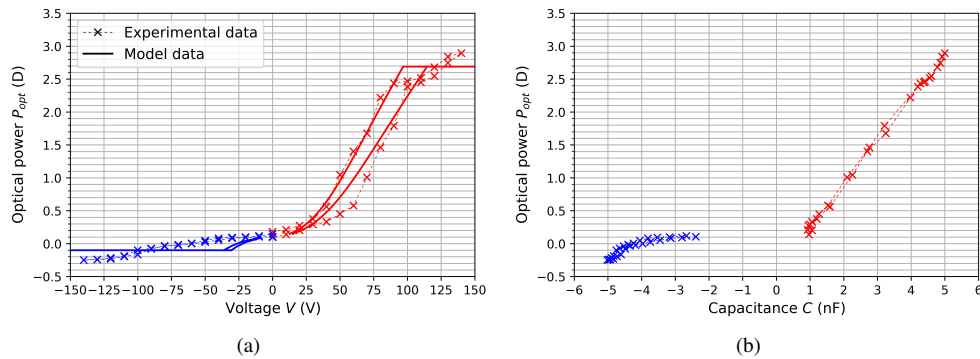


Fig. 6. Typical optical power response of the opto-fluidic engine as a function of voltage (a) and of the capacitance of the actuator (b). Experimental data (dashed lines, with 'x' markers) is presented along with model data (solid lines). The 2 sets of data were acquired through the same acquisition. The voltage course was: first, 0 V to 140 V, then, 140 V to 0 V, then, 0 V to  $-140$  V, last,  $-140$  V to 0 V. Positively noted voltages appear in red, while negatively noted voltages appear in blue.

Figure 6(a) also reveals the presence of voltage hysteresis of about 0.8 D. It comes from the actuator as detailed by Lavigne *et al.* [51]. Hysteresis is quite common and concerns many different types of actuators. The presence of hysteresis makes accurate driving more complex. The easy way out is to get a control parameter which enables to get rid of hysteresis. In our case, the hysteresis of the optical response is nearly totally suppressed when the optical response is regarded as a function of the capacitance of the actuator as illustrated on Fig. 6(b). It was expected as the capacitance monitors the fluid volume, therefore the optical power. More precisely, the figure shows that the hysteresis decreases below 0.2 D, which is not significant as compared to the depth-of-field of the eye.

The model gives a requested maximum voltage of about 110 V. At this voltage, the power consumption of the driver is typically 55 mW.

#### 4.2.2. Dynamic response

The dynamic optical response of the opto-fluidic engine switching between far vision and near vision, undergoing a 3 D power step, is plotted on Fig. 7. Our model predicts an exponential temporal response. Its time constant should be about 1.1 s and its response time, assessed as the time to reach the final value within  $\pm 0.25$  D, should be about  $2.5\tau = 2.7$  s, given the initial lateral tension of the membrane (here 5 N/m) and the expected viscous loss of the opto-fluidic engine (here  $1.5 \times 10^9$  Pa s/m<sup>3</sup>). Experimentally, we observe a temporal response that is close to an exponential decay. The experimental time constant given by the exponential fit is 1.8 s for the ascent and 1.2 s for the descent. The response time on the raw experimental data is about

4.0 s for the ascent and 2.6 s for the descent. It is too long as regards vision comfort. As the lateral tension is here about 5 N/m at 0 D and 9 N/m at 3 D, we cannot really rely on the simple modeling of Eq. (6) and a more accurate model is needed. Additionally, we notice an unexpected asymmetry between both directions, which is not taken into account in this simple linear model. The course of the lateral tension through the membrane deformation being different (opposite) whether in the divergence process or in the convergence process may account for this asymmetry.

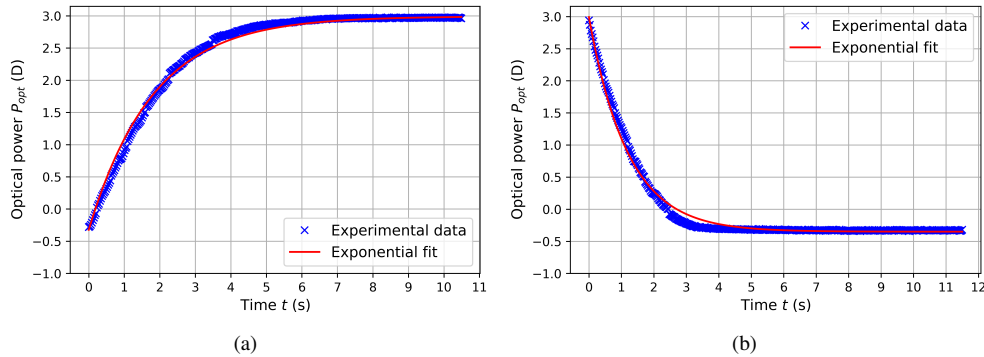


Fig. 7. Typical dynamic optical power response of the opto-fluidic engine in the plano configuration, switching from far vision to near vision (a) and from near vision to far vision (b), under a voltage step from  $-140$  V to  $140$  V and from  $140$  V to  $-140$  V, respectively.

#### 4.2.3. Optical quality

A qualitative analysis of the optical quality of the lens was conducted using a resolution test chart - USAF Resolving Power Test Target 1951 (Edmund). We used an artificial eye composed of a high resolution camera (Edmund Optics EO-5012C) and a short lens (Edmund Optics 25 mm) with an adjustable aperture covering 6 stops. Our variable-focus lens was placed vertically right after the camera lens (as close as possible to the camera lens) and was roughly centered with respect to the aperture hole. We considered an aperture of  $f/5.6$  corresponding to a pupil diameter of 4.5 mm. The images of the test chart obtained with the artificial eye, alone and through the variable-lens, are presented for far vision on Fig. 8 and for near vision on Fig. 9. We were limited by the imaging performance of the artificial eye so we cannot conclude on the imaging performance of the variable-focus lens. Indeed, the maximum spatial frequency that we can observe is the same either with and without the variable lens: around group 0 element 3 for far vision, which corresponds to an angle of resolution of 0.13 mrad, and, around group 2 element 2 for near vision, which corresponds to an angle of resolution 0.34 mrad. Still, these images show us that the lens quality is well beyond the specifications given by classic eye charts for far vision (0.29 mrad MAR, MAR standing for Minimum Angle of Resolution, according to Monoyer Chart) and near vision (0.44 mrad MAR according to Parinaud chart).

## 5. Discussion

### 5.1. Optimization of the actuation pressure and of the electrical consumption

In the experimental configuration presented on Fig. 5, which corresponds to the plano configuration, the requested actuation pressure range only spans over positive differential pressures; it is about [0, 200 Pa]. This configuration does not take advantage of the actuator also being able

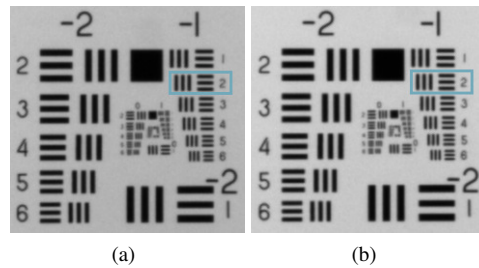


Fig. 8. Imaging of the resolution test chart in far vision with the artificial eye through the variable lens (a) and alone (b). Far vision was assessed at 3 m, the focus was adjusted with the lens camera so that we could analyze the optical quality of the variable-focus lens at 0 D. The focus was manually adjusted, so it is probably not exactly the best focus. The pattern closest to the distance vision specification (10/10) given by the Monoyer chart (0.29 mrad MAR equivalent to 0.57 c/mm at 3 m) is highlighted by the blue box (group -1 element 2). The acquisition parameters are the same for the 2 images. One can note a decrease in the transmission when adding our lens since our lens is not featuring anti-reflection coatings here.

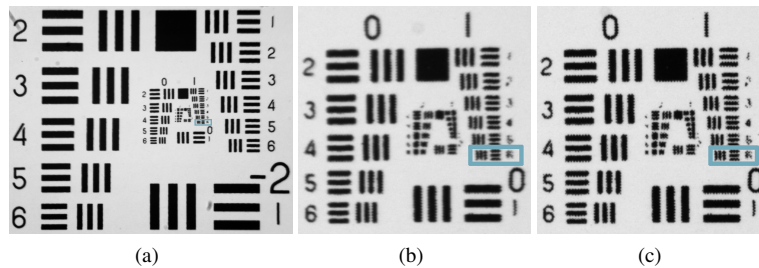


Fig. 9. Imaging of the resolution test chart in near vision with the artificial eye through the variable lens (a)/(b) and alone (c). Image (b) shows a magnification of the central part of image (a). Near vision was assessed at 33 cm, the focus was done with the variable-focus lens on image (a)/(b) - the lens camera focus being adjusted to infinity - and with the lens camera on image (c). The focus was manually adjusted, so it is probably not exactly the best focus. The pattern closest to the near vision specification (0.44 mrad MAR equivalent to 3.4 c/mm at 3 m) is highlighted by the blue box (group 1 element 6).

to deliver the opposite negative differential pressures ( $[-200 \text{ Pa}, 0]$ ) without consuming more energy.

In practice, ophthalmic lenses are not plano - there are a few exceptions. When the lens is curved, the lens rest state (where the membrane is plane) features a positive offset power (cf. Fig. 1(b)). As long as this offset power is inferior to the target near vision addition, both negative and positive actuation pressures are used to provide the required addition range thus the maximum actuation pressure is reduced as compared to the plano configuration, that is why the curved configuration is beneficial in terms of electrical consumption - as expressed by Eq. (4), the less the actuation pressure, the less the voltage.

For a given refractive index difference, there is an optimal configuration, an optimal base curve, where the maximum requested actuation pressure (in absolute terms) is minimal, thus where the peak electrical consumption is minimal. In the optimal base curve configuration, the deformation

range of the membrane that is used to provide the requested addition range is symmetrical to the rest state position of the membrane and the actuation pressure range is symmetrical to 0 Pa. This configuration is all the more favorable in terms of electrical consumption that the actuation pressure is a cubic function of the optical power, so for a given amplitude of the actuation pressure range, the largest optical power range is provided when centered around 0 Pa. It is also interesting to note that the rest position of the membrane in this optimal configuration which is at the middle of the requested addition range (3 D) corresponds roughly to intermediate vision ( $3D/2 = 1.5D$ ) for an absolute presbyope. Knowing that people spend more and more time in intermediate vision, this is very beneficial as no energy is consumed in the rest state.

Considering the experimental parameters of the lens presented above on Fig. 5, we show on Fig. 10, the optical response of the opto-fluidic engine on the one hand in the plano configuration and on the other hand in the optimal curved configuration, for different values of refractive index. For a 0.2 refractive index difference (our experimental configuration), the maximum requested actuation pressure to obtain the [0, 3 D] addition range goes from  $\sim 200$  Pa in the plano configuration to  $\sim 70$  Pa in the optimal configuration, where the radius of curvature of the adaptive doublet lens is 133 mm, which converts to a base curve of 4 D. The requested actuation pressure to provide the [0, 3 D] addition as a function of the base curve is summarized on Fig. 11.

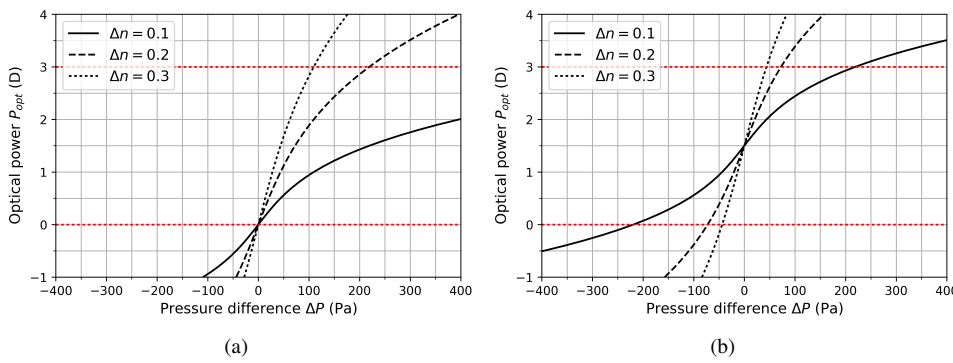


Fig. 10. Optical power response of the opto-fluidic engine as a function of the actuation pressure for several values of refractive index difference in the plano configuration (a) and in the optimal curved configuration (b). The red dotted lines enable to enclose the necessary actuation pressure range to provide the [0, 3 D] power range.

In our experiment, the base curve is 0 D. In order to characterize the optical response we would have in the optimal base curve configuration, we have to work around 0 D, from  $-1.5$  D to  $1.5$  D. To do that, we adjust the volume of each liquid so that  $-1.5$  D can be obtained for the extremal voltage. The requested offset power would then be  $1.5$  D which would make the power come to 0 to 3 D. The resulting experimental power (corrected with the offset power) is given on Fig. 12. The model gives a maximum requested voltage of about 80 V which leads to a power consumption of about 25 mW. The power consumption is less than half the one required in the plano configuration.

### 5.2. Optimization of the response time

As for Fig. 12, we worked around 0 D from  $-1.5$  D to  $1.5$  D to assess the dynamic response we would have in the optimal configuration. The resulting dynamic response (corrected with the offset power) is given on Fig. 13. Here the additional lateral tension of the membrane at 3 D is low (about 1 N/m) so the comparison with the model is more relevant. We are very close to

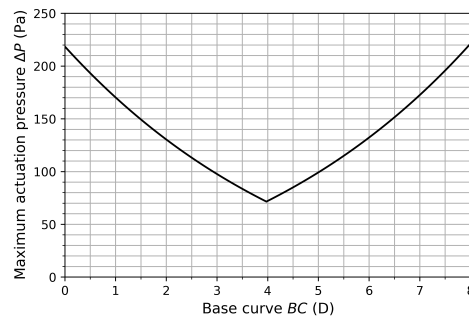


Fig. 11. Maximum actuation pressure as a function of base curve for a 0.2 refractive index difference. The offset power was computed as  $\Delta n/(n_{ref} - 1) \cdot BC$  with  $BC$  the base curve and  $n_{ref} = 1.530$  the standard reference refractive index.

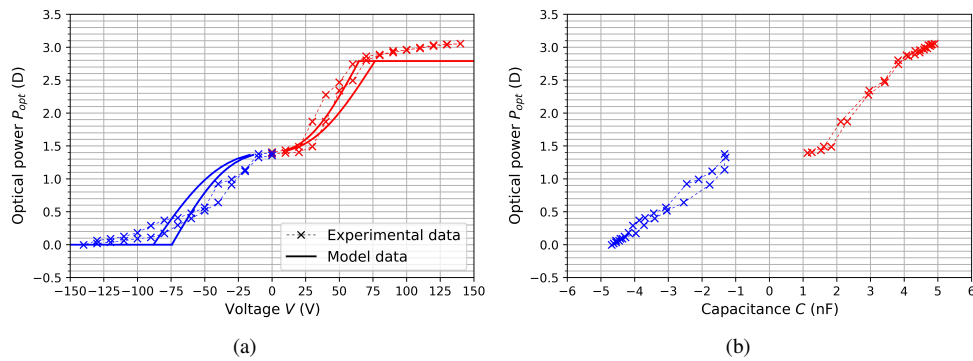


Fig. 12. Typical optical power response of the opto-fluidic engine in the optimal base curve configuration, as a function of voltage (a) and of the capacitance of the actuator (b). Experimental data (dashed lines, with 'x' markers) is presented along with model data (solid lines). The 2 sets of data were acquired through the same acquisition. The voltage course was: first, 0 V to 140 V, then, 140 V to 0 V, then, 0 V to -140 V, last, -140 V to 0 V. Positively noted voltage appear in red, while negatively noted voltage appear in blue.

the model described by Eq. (6). For the ascent, illustrated on Fig. 13(a), the curves are nearly perfectly superimposed. The experimental time constants are 1.1 s for the ascent and 1.5 s for the descent. The response times are 2.3 s and 3.4 s for the ascent and descent, respectively. It has to be noticed that the applied voltage here (the maximum voltage: 140 V) is well above the precise value of the requested driving voltage to provide for the 3 D variation (about 80 V according to the model, cf. Sect 5.1) and that this tends to speed up the response time. In the optimal configuration, the values taken by the lateral tension are exactly the same whether going from 0 to 3 D or the reverse, so we expected the same response time for the ascent and the descent. However, these are slightly asymmetric. The model has still to be refined to explain these differences.

The response time remains a little long, even though first testers did not point out this drawback and even though the response is faster here, in the optimal configuration that is centered around 0 Pa. We are considering several upgrades for the next generation of prototypes, aiming at a response time of 1 s (cf. Sect. 2.3). Possibilities of improvement include choosing less viscous liquids, modifying the design of the lens channels and the design of the actuator. The detailed

contributions of the constituting components to the fluidic impedance here are  $7.5 \times 10^8 \text{ Pa s/m}^3$  for the actuator,  $6.8 \times 10^8 \text{ Pa s/m}^3$  for the lens and  $5.0 \times 10^7 \text{ Pa s/m}^3$  for the connectors. This emphasizes that further progress will rely both on the lens and on the actuator design changes, as their relative contributions are roughly balanced. In the optimal configuration, the maximum actuation pressure requires a voltage lower than the maximum voltage that can be delivered by the drivers so we could also take advantage of overshoot driving to accelerate the response.

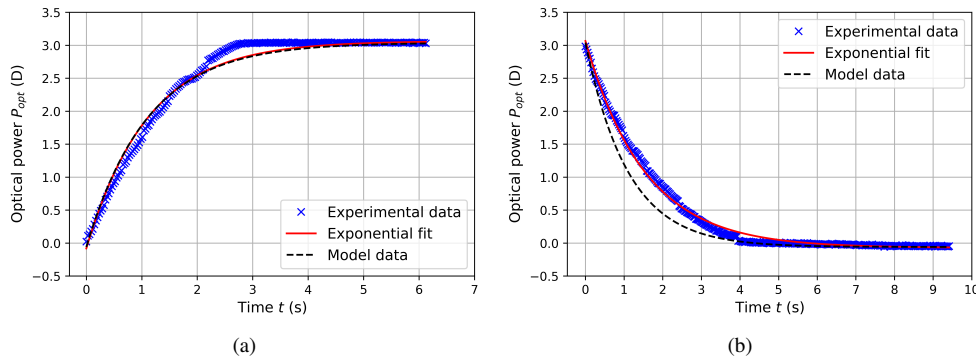


Fig. 13. Typical dynamic power response of the opto-fluidic engine in the optimal curved configuration, switching from far vision to near vision (a) and from near vision to far vision (b), under a voltage step from  $-140 \text{ V}$  to  $140 \text{ V}$  and from  $140 \text{ V}$  to  $-140 \text{ V}$ , respectively. Experimental data (blue 'x' markers) is presented along with model data (black dashed lines) and fit data (red solid lines).

### 5.3. Optimization of the ergonomics: better assessment of the focusing distance, less head movements

The open loop control system implemented here to control the actuation pressure and the lens optical power is based on the measurement of the focusing distance of the wearer by an ultrasonic sensor. This distance sensor is bulky and its field-of-view is very large. An ultra-compact infrared LIDAR is currently being integrated to replace this US sensor. This solution is relevant. However, when the scene includes objects closer to the wearer than the target object, the sensor can mislead. These situations make the user switch to manual mode, which provides the addition for a few selected distances of focus. So as to minimize the failure rate of such an automatic mode, the sensing field ought not to be too large, which implies relying on the head moving of the wearer.

A further step would be to use a multizone LIDAR combined with a low-resolution CMOS camera pointing toward the eye [55], as shown on Fig. 14. The aim would be to get the distance measurement in the gaze direction, which would contribute to significantly enhance the ergonomics as the wearer would be able to point off axis targets without moving the head and to deal with complex scene (with different object depths across the sensing field). To do so, the pupil camera would provide the gaze direction and the distance of interest would then be assessed in the corresponding zone of the multizone LIDAR.

The variable zone is 20 mm wide. This value was set considering specifications detailed in Sect. 2.4. So as to enhance the field-of-view at close distances, which could be appealing for eye-movers (people who tend to accomplish gaze shifts with a lesser contribution from head movements [56]), the size of the variable zone could be enlarged by increasing the refractive index difference or increasing the volume that the actuator can displace (see Fig. 2).

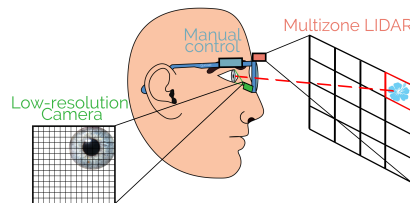


Fig. 14. Setting up a multizone LIDAR combined with a low-resolution camera in the frame of the eyeglasses to enhance ergonomics. The low-resolution camera is pointing toward the eye of the wearer in order to determine the gaze direction and the multizone LIDAR is providing a distance map.

#### 5.4. Optimization of the power control

As shown in Sect. 4.2.1, the control system would benefit from a feedback loop on the capacitance of the actuator. Indeed, such a control would enable to bypass the hysteresis of the actuator, thus greatly decrease the error on the output power, as the capacitance is a good indicator of the lens power. The control would still rely on a calibration table, which would then state the optical power as a function of the capacitance.

#### 5.5. Optimization of the aesthetics

The presented prototype was developed to demonstrate the potential of our opto-fluidic technology but is far from looking like a genuine prototype of eyeglasses. Several upgrades are planned for the coming generation. The pump is currently  $55 \times 18 \times 7 \text{ mm}^3$  but its active volume is  $45 \times 8 \times 70.3 \text{ mm}^3$  [51], so there is room for miniaturization. The US sensor is very bulky but the LIDAR sensor is just a few square millimeters, and can be set behind a plastic cover, in the eyeframe. Also, the interface between the lens and the pump has to be designed to fit nicely in the eyeframe. Regarding the lens, the prototype exhibits plano lenses here, whereas standard ophthalmic lenses are curved (for both aesthetics and optical quality). Our next generation of prototypes will be equipped with curved lenses with custom contours and benefit from standard optical treatments. The lens could also be made thinner, thinner than 1 mm for a 0.2 refractive index difference, as shown by Fig. 2.

### 6. Conclusion

We have presented a new opto-fluidic technology for presbyopia-correcting adaptive eyeglasses. Through a theoretical and experimental analysis, we showed the viability of this technology as regards the optical, aesthetics and portability requirements on such eyeglasses. The key features are, first, its soft actuation technology enabling to get the necessary 3-diopter-high power variation with low energy, and second, its lens design.

A prototype featuring a 20-millimeter-wide diameter variable zone and plano lenses was set up. We demonstrated that it was fully functional. This is a good achievement as the plano configuration is the worst case scenario in terms of membrane deformation and requested actuation pressure, while ophthalmic lenses are (almost) never plano. The prototype meets the requirements in terms of addition range ( $[0, 3 \text{ D}]$ ). It operates with a maximum actuation pressure of  $\sim 200 \text{ Pa}$  which is provided by low-power custom-designed actuators. The power control is automatic and a control system based on capacitance monitoring yields to a negligible power error ( $<0.2 \text{ D}$ ). Its response time is reasonable; yet, it was a little under-specified as compared to the natural accommodative response. Last, the qualitative visual tests that we carried out on this prototype did not highlight any limitations in terms of optical quality and showed lens quality is well beyond the optical specifications given by eye charts.

This variable-focus technology is compatible with the standard range of base curves used for ophthalmic lenses. Besides, we demonstrated that it features an optimal base curve configuration in terms of energy efficiency where the membrane symmetrically moves back and forth around its rest position (plane). For a 0.2 refractive index difference, this base curve is 4 D (which is a commonly used base curve). The maximum actuation pressure then drops to  $\sim 70$  Pa, leading to a reduced energy consumption, with a peak consumption divided by 2 at least as regards the plano configuration and amounting to  $\sim 25$  mW.

To conclude, this technology has the potential to become a serious alternative to current corrective solutions for presbyopes. We are now developing the next generation of prototypes which will be faster and significantly lighter. It will integrate curved customized lenses, a miniaturized actuator as well as a miniature LIDAR to sense the focusing distance.

## Funding

Bpifrance grant i-Lab 2017.

## Acknowledgments

The authors are grateful to the INL - Lyon Institute of Nanotechnology and to the ENS de Lyon, and also to its supporters, especially Incubateur Voir et Entendre and Pulsalsys.

## References

1. F. C. Donders, *On the anomalies of accommodation and refraction of the eye* (The New Sydenham Society, 1864).
2. D. Hamasaki, J. Ong, and E. Marg, "The amplitude of accommodation in presbyopia," *Am. J. Optom. Arch. Am. Acad. Optom.* **33**(1), 3–14 (1956).
3. A. Duane, "Studies in monocular and binocular accommodation, with their clinical application," *Trans. Am. Ophthalmol. Soc.* **20**, 132–157 (1922).
4. T. R. Fricke, N. Tahhan, S. Resnikoff, E. Papas, A. Burnett, S. M. Ho, T. Naduvilath, and K. S. Naidoo, "Global prevalence of presbyopia and vision impairment from uncorrected presbyopia: systematic review, meta-analysis, and modelling," *Ophthalmology* **125**(10), 1492–1499 (2018).
5. B. P. Luo, G. C. Brown, S. C. Luo, and M. M. Brown, "The quality of life associated with presbyopia," *Am. J. Ophthalmol.* **145**(4), 618–622 (2008).
6. P. J. McDonnell, P. Lee, K. Spritzer, A. S. Lindblad, and R. D. Hays, "Associations of presbyopia with vision-targeted health-related quality of life," *Arch. Ophthalmol.* **121**(11), 1577–1581 (2003).
7. C. Y. Chen, J. E. Keeffe, P. Garoufalidis, F. M. A. Islam, M. Dirani, T. A. Couper, H. R. Taylor, and P. N. Baird, "Vision-related quality of life comparison for emmetropes, myopes after refractive surgery, and myopes wearing spectacles or contact lenses," *J. Refract. Surg.* **23**(8), 752–759 (2007).
8. W. N. Charman, "Developments in the correction of presbyopia I: spectacle and contact lenses," *Ophthalmic Physiol. Opt.* **34**(1), 8–29 (2014).
9. Y. Benard, A. Seidemann, H. Altheimer, A. Welk, and G. Esser, "Reducing prismatic imbalance at near in progressive addition lenses," *Investig. Ophthalmol. Vis. Sci.* **59**(9), 2967 (2018).
10. D. J. Meister and S. W. Fisher, "Progress in the spectacle correction of presbyopia. Part 2: Modern progressive lens technologies," *Clin. Exp. Optom.* **91**(3), 251–264 (2008).
11. L. Bonnin and V. Torrilhon, "Study on the satisfaction of people who wear progressive lenses, conducted in optical stores," (Points de Vue, 2018). <https://www.pointsdevue.com>
12. S. C. Han, A. D. Graham, and M. C. Lin, "Clinical assessment of a customized free-form progressive add lens spectacle," *Optom. Vis. Sci.* **88**(2), 234–243 (2011).
13. J. Forkel, J. L. Reiniger, A. Muschielok, A. Welk, A. Seidemann, and P. Baumbach, "Personalized progressive addition lenses: correlation between performance and design," *Optom. Vis. Sci.* **94**(2), 208–218 (2017).
14. E. Chamorro, J. M. Cleva, P. Concepcion, M. S. Subero, and J. Alonso, "Lens design techniques to improve satisfaction in free-form progressive addition lens users," *JOJ Ophthalmol.* **6**(3), 555688 (2018).
15. J. E. Sheedy, C. Campbell, E. King-Smith, and J. R. Hayes, "Progressive powered lenses: the Minkwitz theorem," *Optom. Vis. Sci.* **82**(10), 916–922 (2005).
16. D. J. Meister and S. W. Fisher, "Progress in the spectacle correction of presbyopia. Part 1: Design and development of progressive lenses," *Clin. Exp. Optom.* **91**(3), 240–250 (2008).
17. T. L. Alvarez, E. H. Kim, and B. Granger-Donetti, "Adaptation to progressive additive lenses: potential factors to consider," *Sci. Rep.* **7**, 2529 (2017).

18. Y. Han, K. J. Ciuffreda, A. Selenow, and S. R. Ali, "Dynamic interactions of eye and head movements when reading with single-vision and progressive lenses in a simulated computer-based environment," *Investig. Ophthalmol. Vis. Sci.* **44**(4), 1534–1545 (2003).
19. W. Jaschinski, M. König, T. M. Mekontso, A. Ohlendorf, and M. Welscher, "Comparison of progressive addition lenses for general purpose and for computer vision: an office field study," *Clin. Exp. Optom.* **98**(3), 234–243 (2015).
20. B. Cagnie, K. De Meulemeester, L. Saeyns, L. Danneels, L. Vandebulcke, and B. Castelein, "The impact of different lenses on visual and musculoskeletal complaints in VDU workers with work-related neck complaints: a randomized controlled trial," *Environ. Health Prev. Med.* **22**(1), 1–8 (2017).
21. J. E. Sheedy, "Progressive addition lenses—matching the specific lens to patient needs," *Optometry* **75**(2), 83–102 (2004).
22. R. Graham, "A variable focus lens and its uses," *J. Opt. Soc. Am.* **30**(11), 560–563 (1940).
23. J. D. Silver, C. Miksovsky, M. Newbery, and A. Robertson, "Variable focus lens," WIPO patent WO/2007/049058 (May 3, 2007).
24. S. Kurtin and S. Epstein, "Spectacles using variable focal length lenses which have an arbitrarily shaped periphery," WIPO patent WO/1995/027912 (October 19, 1995).
25. N. Hasan, A. Banerjee, H. Kim, and C. H. Mastrangelo, "Tunable-focus lens for adaptive eyeglasses," *Opt. Express* **25**(2), 1221–1233 (2017).
26. L. Wang, H. Oku, and M. Ishikawa, "Variable-focus lens with 30 mm optical aperture based on liquid-membrane-liquid structure," *Appl. Phys. Lett.* **102**, 131111 (2013).
27. Y. Lo and D. Zhang, "Fluidic adaptive lens," WIPO patent WO/2006/011937 (February 2, 2006).
28. S. Kuiper and B. H. W. Hendriks, "Variable focus spectacles," WIPO patent WO/2005/003842 (January 13, 2005).
29. L. W. Alvarez, "Two-element variable-power spherical lens," U.S. patent 3,305,294 (February 21, 1967).
30. J. Nisper and R. E. Stevens, "Variable-power lens," WIPO patent WO/2014/124707 (August 21, 2014).
31. A. F. Naumov, M. Y. Loktev, I. R. Guralnik, and G. Vdovin, "Liquid-crystal adaptive lenses with modal control," *Opt. Lett.* **23**(13), 992–994 (1998).
32. G. Li, D. L. Mathine, P. Valley, P. Åyräs, J. N. Haddock, M. S. Giridhar, G. Williby, J. Schwiegerling, G. R. Meredith, B. Kippelen, S. Honkanen, and N. Peyghambarian, "Switchable electro-optic diffractive lens with high efficiency for ophthalmic applications," *Proc. Natl. Acad. Sci.* **103**(13), 6100–6104 (2006).
33. Y. Yadin, A. Alon, and Y. Haddad, "Lenses with electrically-tunable power and alignment," WIPO patent WO/2014/049577 (April 3, 2014).
34. M. Millodot and S. Millodot, "Presbyopia correction and the accommodation in reserve," *Ophthalmic Physiol. Opt.* **9**(2), 126–132 (1989).
35. D. Meslin, *Practical refraction* (Essilor Academy Europe, 2008).
36. J. S. Wolffsohn, A. L. Sheppard, S. Vakani, and L. N. Davies, "Accommodative amplitude required for sustained near work," *Ophthalmic Physiol. Opt.* **31**(5), 480–486 (2011).
37. H. W. Hofstetter, "A longitudinal study of amplitude changes in presbyopia," *Am. J. Optom. Arch. Am. Acad. Optom.* **42**(1), 3–8 (1965).
38. W. N. Charman, "The eye in focus: accommodation and presbyopia," *Clin. Exp. Optom.* **91**(3), 207–225 (2008).
39. E. Chirre, P. Prieto, and P. Artal, "Dynamics of the near response under natural viewing conditions with an open-view sensor," *Biomed. Opt. Express* **6**(10), 4200–4211 (2015).
40. G. Heron and B. Winn, "Binocular accommodation reaction and response times for normal observers," *Ophthalmic Physiol. Opt.* **9**(2), 176–183 (1989).
41. M. Bass, C. De Cusatis, J. Enoch, V. Lakshminarayanan, G. Li, C. MacDonald, V. Mahajan, and E. V. Stryland, *Handbook of optics, third edition, volume III* (McGraw Hill Professional, 2009).
42. The 2015 digital eye strain report, "Hindsight is 20/20: protect your eyes from digital devices" (The Vision Council, 2015). <https://www.thevisioncouncil.org/blog/2015-digital-eye-strain-report-released>
43. D. Paillé, "Impact of new digital technologies on posture," *Points de Vue* **72**, 22–30 (2015).
44. W. Jaschinski, "The proximity-fixation-disparity curve and the preferred viewing distance at a visual display as an indicator of near vision fatigue," *Optom. Vis. Sci.* **79**(3), 158–169 (2002).
45. D. Ankrum, "Viewing distance at computer workstations," *Workplace Ergonomics* **2**(5), 10–13 (1996).
46. D. J. Meister and J. E. Sheedy, *Introduction to ophthalmic optics* (SOLA Optical, 1999).
47. M. Cohen, O. Antonshyn, and A. Michaeli-Cohen, "Spectacle-induced nasal dermochalasis—a new entity," *Eur. J. Plast. Surg.* **26**(7), 335–337 (2003).
48. G. C. Knollman, J. L. S. Bellin, and J. L. Weaver, "Variable-focus liquid-filled hydroacoustic lens," *J. Acoust. Soc. Am.* **49**(1B), 253–261 (1971).
49. M. S. Ober, D. Dermody, M. Maillard, F. Amiot, G. Malet, B. Burger, C. Woelfle-Gupta, and B. Berge, "Development of biphasic formulations for use in electrowetting-based liquid lenses with a high refractive index difference," *ACS Comb. Sci.* **20**(9), 554–566 (2018).
50. B. Berge, "Electrostatically actuated device," WIPO patent WO/2018/041866 (March 8, 2018).
51. Q. Lavigne, N. Terrier, G. Noetinger, D.-D. Tran, S. Kulifaj, P. Kleimann, P. Pittet, and B. Berge, "Novel concept of a low-power high-volume microfluidic actuator: theory of operation and experimental characterization," *Sens. Actuator A-Phys.* (to be published).
52. N. R. Fong, P. Berini, and R. N. Tait, "Mechanical properties of thin free-standing CYTOP membranes," *J.*

- Microelectromech. Syst. **19**(3), 700–705 (2010).
53. J.-L. Wang, T.-Y. Chen, Y.-H. Chien, and G.-D. J. Su, “Miniature optical autofocus camera by micromachined fluoropolymer deformable mirror,” Opt. Express **17**(8), 6268–6274 (2009).
54. B. Berge, “Ophthalmic lens with dynamic focus control,” WIPO patent WO/2018/007425 (January 11, 2018).
55. J. Jarosz, Q. Lavigne, N. Molliex, G. Chenon, G. Noettinger, D.-D. Tran, and B. Berge, “Experimental optical analysis of an original presbyopia-correcting variable focus lens,” Investig. Ophthalmol. Vis. Sci. **59**(9), 255 (2018).
56. P. A. Aitsebaomo and J. A. Afanador, “Contribution of eye and head movement for a near task,” Am. J. Optom. Physiol. Opt. **59**(11), 863–869 (1982).